Journal of Catalysis **190,** 374–386 (2000)
doi:10.1006/jcat.1999.2754, available online at http://www.idealibrary.com on IDEAL®

The Effect of the Pore Structure of Medium-Pore Zeolites on the Dehydroisomerization of *n*-Butane: A Comparison of Pt–FER, Pt–TON, and Pt–ZSM5

G. D. Pirngruber, O. P. E. Zinck-Stagno, K. Seshan, and J. A. Lercher[1]

Faculty of Chemical Technology, University of Twente, P.O. Box 217, 7500 AE Enschede, The Netherlands

Received August 1, 1999; revised October 28, 1999; accepted November 2, 1999

The catalytic dehydroisomerization of *n*-butane over Pt–ZSM5, Pt–TON, and Pt–FER was investigated. Pt–ZSM5 showed the highest yield and selectivity to isobutene. Most of the by-products of Pt–ZSM5 were formed by oligomerization/cracking of butene, while acid-catalyzed cracking and metal-catalyzed hydrogenolysis of *n*-butane were more pronounced with Pt–TON and especially with Pt–FER. Skeletal isomerization of butene and cracking of *n*-butane are both acid catalyzed. But as the rate of *n*-butane cracking depends more strongly on the concentration of acid sites than the rate of butene isomerization, low acid site concentrations are beneficial for dehydroisomerization catalysts. The dehydrogenation activity of the Pt–zeolites is not only related to the concentration of accessible metal sites. Pt–FER had the highest dispersion, but the lowest dehydrogenation activity. This is attributed to diffusional constraints in the narrow pores of the large ferrierite crystals. © 2000 Academic Press

Key Words: **dehydroisomerization of *n*-butane; 10-membered-ring zeolites; bifunctional catalysis.**

INTRODUCTION

The dehydroisomerization of *n*-butane requires a bifunctional catalyst comprising a metal function for dehydrogenation of *n*-butane to *n*-butenes and an acid function for isomerizing the *n*-butenes to isobutene. Side reactions are protolytic cracking of *n*-butane and oligomerization/cracking of butene on acid sites and hydrogenolysis on the metal. Recently, we reported that Pt–ZSM5 can be successfully used as a catalyst for the direct conversion of *n*-butane to isobutene (1). Protolytic cracking of *n*-butane and hydrogenolysis played only a minor role with Pt–ZSM5, making the catalyst very selective at low conversion levels. A sharp increase in selectivity to oligomerization/cracking reactions of butenes was, however, observed as the ratio of isobutene to the sum of butenes approached thermodynamic equilibrium.

The rather high selectivity of ZSM5 to oligomerization/cracking is inherent to H–ZSM5 and was attributed to the fact that the pore intersections of ZSM5 are too large to prevent the formation of bulky oligomers that crack easily (2). This severely limits the potential of Pt–ZSM5 as a catalyst for the dehydroisomerization of *n*-butane. Better results should be achieved by using other microporous materials that have a higher selectivity to butene isomerization vs oligomerization/cracking than ZSM5. Several such catalysts have been successfully used for the skeletal isomerization of butene, e.g., FER (3–5), TON (6, 7), ZSM-23 (8), SAPO-11 (9), MeAPOs (10), MCM22 (11), etc. From these, the zeolites TON and FER were chosen. For both materials excellent selectivities in butene isomerization have been reported in patent literature (12, 13). The framework of each is sufficiently stable for use at the high temperatures necessary for dehydroisomerization.

The objective of the work described here was to explore whether the good catalytic performance of FER and TON in skeletal isomerization of butene can be combined with a dehydrogenating component to obtain superior catalysts for the dehydroisomerization of *n*-butane than Pt–ZSM5. The results obtained are discussed in terms of the effect of the zeolite structure, the acid site concentration, and the concentration of accessible metal sites on the catalytic performance.

EXPERIMENTAL

Catalyst Preparation

ZSM5 ($SiO_2/Al_2O_3 = 480$) was received from ZEOLYST Int. (sample code CBV10002). K–FER with a SiO_2/Al_2O_3 ratio of 17 was provided by TOSOH. In order to obtain the ammonium form, the sample was ion-exchanged three times for 12 h at room temperature with 1 M NH_4NO_3 solution. Two FER samples, with SiO_2/Al_2O_3 ratios of 90 and 670, respectively, were provided by Exxon Chemicals Europe. FER(90) was received in the as-synthesized form. In order to remove the template, the sample was calcined

[1] Present address: Institute for Chemical Technology, Technische Universität München, Lichtenbergstr. 4, D-85748 Garching, Germany.

0021-9517/00 $35.00

TABLE 1

Physico-chemical Characterization of the Samples

Sample	Pt-loading (wt%)	SiO_2/Al_2O_3	Al (mmol/g)	(L + B) (mmol/g)		L/(L + B) (%)	
				parent	Pt	parent	Pt
ZSM5(480)	0.09	480	0.07	n.d.[a]	0.05	n.d.	38
FER(17)	0.10	17	1.79	1.7	1.65	4	7
	0.31	19	1.59	1.7	n.d.	4	n.d.
FER(90)	0.10	89	0.37	0.45	n.d.	4	n.d.
FER(670)	0.10	670	0.05	n.d.	n.d.	n.d.	n.d.
TON(35)	0.11	35	0.92	0.4	0.5	23	26
TON(72)	0.09	72	0.45	0.25	n.d.	17	n.d.

Note: SiO_2/Al_2O_3 ratio, Al content, and Pt content were determined by XRF; the total concentration of acid sites and the ratio of Lewis acid sites (L) to the total number of acid sites (L + B) were determined by adsorption of pyridine (IR).

[a] n.d. = not determined.

for 2 h at 798 K (temperature increment 2 K/min) in N_2, then cooled to 573 K, and finally calcined in air at 798 K (temperature increment 2 K/min) for 4 h. The template-free zeolite was ion-exchanged three times with 1 M NH_4NO_3 solution in the same way as described above. FER(670) was already received in the ammonium form.

Mg–TON ($SiO_2/Al_2O_3 = 35$) was received from Exxon Chemicals Europe. In order to obtain the ammonium form, the sample was ion-exchanged two times with 1 M NH_4NO_3 solution and once with 0.01 M NH_4NO_3 solution (each time for about 12 h). NH_4–TON with a SiO_2/Al_2O_3 of 72 (synthesized according to the procedure described in Ref. 14) was received from G. Kinger, TU Vienna.

Pt was incorporated by slow addition of a dilute aqueous solution of $Pt(NH_3)_4(OH)_2$ (0.1 mg of Pt/l) and NH_3 (~2%) to a suspension of the zeolite in doubly distilled water (10 ml of H_2O/g of zeolite) (1). After being stirred for 12 h the sample was filtered and dried. Subsequently, it was calcined at either 523 or 723 K (temperature increment 0.5 K/min) in air for 2 h and pre-reduced at either 673 or 773 K (temperature increment 5 K/min) in H_2 for 2 h. Because the catalysts were reduced *in situ* at even higher temperatures (1 h at 823 K) before use in the reaction, the choice of the calcination procedure did not affect the catalytic behavior.

The samples were characterized by X-ray fluorescence (determination of the elemental composition) and pyridine adsorption (determination of the concentration of Lewis and Brønsted acid sites) (15). The results are compiled in Table 1. In the following text the SiO_2/Al_2O_3 ratio of the samples is indicated in parentheses at the end of the name. The morphology of the samples was determined by SEM (see Table 2).

Catalytic Testing

The catalysts were mixed with about 60 mg of quartz and placed in a quartz reactor of 4 mm inner diameter. Each sample was activated *in situ* in a flow of 25 ml/min H_2/Ar (20/80) at 830 K for 1 h and then cooled to the reaction temperature. The reaction was carried out at 775 K and atmospheric pressure; 775 K was chosen as the reaction temperature in order to minimize catalyst deactivation (16). The reaction was started by switching the reactor inlet to a mixture of 10% *n*-butane, 20% H_2, the balance being Ar. In the first minutes on stream the reactor effluent was stored in sample loops for postrun GC analysis. After 10 min, the reactor effluent was analyzed online in intervals of about 45 min, without making use of the storage loops. An Al_2O_3 PLOT column and a combination of a Hayesep C and a MS5Å column in parallel were used for the separation of H_2 and the hydrocarbons. In general, the measured H_2 production corresponded very well with the stoichiometry of dehydrogenation. $\Delta[H_2]/([C_4^=] + 2[C_4^{==}])$ was always between 0.8 and 1.0. Yields and selectivities of the hydrocarbon products were reported on the basis of mole percent carbon converted.

Characterization of Pt Dispersion and Location

High-resolution electron microscopy (HREM) was applied to study the size and location of the Pt particles. The

TABLE 2

Morphology of the Samples, as Analyzed by SEM

Sample	Morphology
0.1% Pt–ZSM5(480)	Spheres, 1–4 μm
0.1% Pt–FER(17)	Platelets, length 0.5–1.5 μm
FER(90)	Platelets, 6–10 μm (also some smaller ones, down to 2 μm)
0.1% Pt–FER(670)	Platelets, needles, 4 μm
0.1% Pt–TON(35)	Needles, length 1–3 μm, plus smaller particles
0.1% Pt–TON(72)	Needles, length 1 μm, plus smaller particles (0.1–0.2 μm)

measurements were performed on a Phillips CM 30 T electron microscope with a LaB_6 filament as the source of electrons operated at 300 kV. The reduced Pt samples were mounted on a microgrid carbon polymer supported on a copper grid by placing a few droplets of a suspension of ground sample in ethanol on the grid, followed by drying at ambient conditions.

In order to quantify the amount of Pt on the outer surface and in the pores of the zeolite, two test reactions were used: (i) the hydrogenation of 2,4,4-trimethylpent-1-ene (244TMPe) and (ii) the hydrogenation of ethene (17). 244TMPe is too large to enter the pores of 10-membered-ring zeolites (18) and can therefore react only on the outer surface. Ethene, on the other hand, can enter the zeolite channels and its hydrogenation rate should, thus, be a measure of the total accessible metal surface area. For both test reactions, the catalyst was reduced *in situ* at 830 K for 1 h in a flow of 5 ml/min H_2 and 20 ml/min Ar at atmospheric pressure. Afterward, the reactor was cooled to 425 K. Then, over 30 min, the bed was flushed with approximately 20 ml/min of a mixture containing 20% NH_3 in He. Subsequently, weakly bound NH_3 was desorbed for 2 h in a stream of 25 ml/min Ar. The purpose of the NH_3 treatment was to deactivate acid sites, which could catalyze unwanted isomerization reactions of 244TMPe. For ethene, the NH_3 treatment was omitted. Finally, the catalyst was cooled to the reaction temperature. The reaction was started by switching from Ar to the alkene/H_2 feed. The feed composition for ethene hydrogenation was chosen in analogy to Ref. (17), i.e., 3% ethene, 20% H_2, the balance being Ar. The reaction temperature of 273 K was kept constant by use of an ice bath. The catalyst mass was 10 mg, and the total flow was 45 ml/min.

For the hydrogenation of 244TMPe, the feed composition was 0.3% 244TMPe, 88% H_2, the balance being Ar. The reaction temperature was 293 K, the catalyst mass 10 mg, and the total flow 175 ml/min. Both reactions were carried out at atmospheric pressure.

Pt–SiO_2 (0.1 wt% Pt, Aerosil SiO_2 Degussa, SA = 200 m^2/g), prepared according to the method of Benesi *et al.* (19), was used as a reference for the test reactions. Since the silica support is nonporous (20), all Pt in this material was necessarily located on the outer surface.

RESULTS

Characterization of Pt Particle Size and Accessible Pt

For both 0.1 and 0.3% Pt–FER(17), only small Pt particles (0.5–3 nm) were found by high-resolution electron microscopy. The particles were distributed throughout the zeolite and most likely located in the zeolite channel system (Fig. 1a). For 0.1% Pt–FER(90), on the other hand, mainly intermediate size (3–10 nm) Pt particles were found. Some were located at or at least near the outer surface; some were located inside the crystal (Fig. 1b).

The HREM photographs of Pt–TON(35) also showed only small Pt particles (0.5–4 nm), the location of which could not be clearly determined. Some seemed to be located inside, and some outside the zeolite channels. In Pt–TON(72) also mainly small particles were found (1–5 nm). A certain accumulation at the edge of the crystals (see Fig. 1c) indicated that a significant fraction was located on the outer surface.

In contrast to the results obtained with FER and TON, the Pt distribution in ZSM5(480) was very inhomogeneous with respect to particle size and location (Fig. 1d). Large Pt particles (15–45 nm) were found at the external surface of the zeolite, next to small particles inside the channel system. In some areas an accumulation of Pt on the outer surface was observed; in other areas no Pt particles could be found. Additional EDX (energy dispersive analysis of X-rays) analysis also did not show Pt in these areas. Similar results were found for ZSM5(480) with a metal loading of 0.5 wt%.

The general trend observed in the HREM measurements was that the samples with lower SiO_2/Al_2O_3 ratios had smaller Pt particles. This was related to the higher ion-exchange capacity and the resulting better stabilization of Pt ions in these samples.

HREM measures only a small fraction of the sample and gives only qualitative information on the dispersion and location of the metal. Thus, test reactions were used to quantify the concentration of accessible Pt located on the outer surface and in the pores of the zeolite. The rate of hydrogenation of 244TMPe, which is too large to enter the pores of 10-membered-ring zeolites (18), was used to assess the concentration of Pt on the outer surface of the zeolite. Ethene, on the other hand, can easily diffuse into the zeolite pores. When measured in the absence of transport limitations, its hydrogenation rate is representative for the total concentration of accessible Pt, since hydrogenation of alkenes is a structure-insensitive reaction (17, 21, 22). The hydrogenation activities are reported in Table 3.

Pt–FER(17) had an extraordinarily high activity for the hydrogenation of ethene. In order to check whether this high activity was related to the high acid site concentration of Pt–FER(17) (1.7 mmol/g), we measured two Pt–ZSM5 samples of different acid site concentrations (0.05 and 0.26 mmol/g, respectively). The two ZSM5 samples gave similar activities for the hydrogenation of ethene. This suggests that sorption on the acid sites affects the observed reaction rates if the acid site concentration is very high, but has little effect on samples of lower acid site density. We therefore believe that—with the exception of Pt–FER(17)—the ethene hydrogenation rate correctly represents the metal dispersion. Absolute dispersion values calculated from these data using turnover frequencies given in Ref. (17) are on the order of 100% and above. The turnover frequencies in Ref. (17) were, however, determined from steady-state activities, while we preferred to use initial

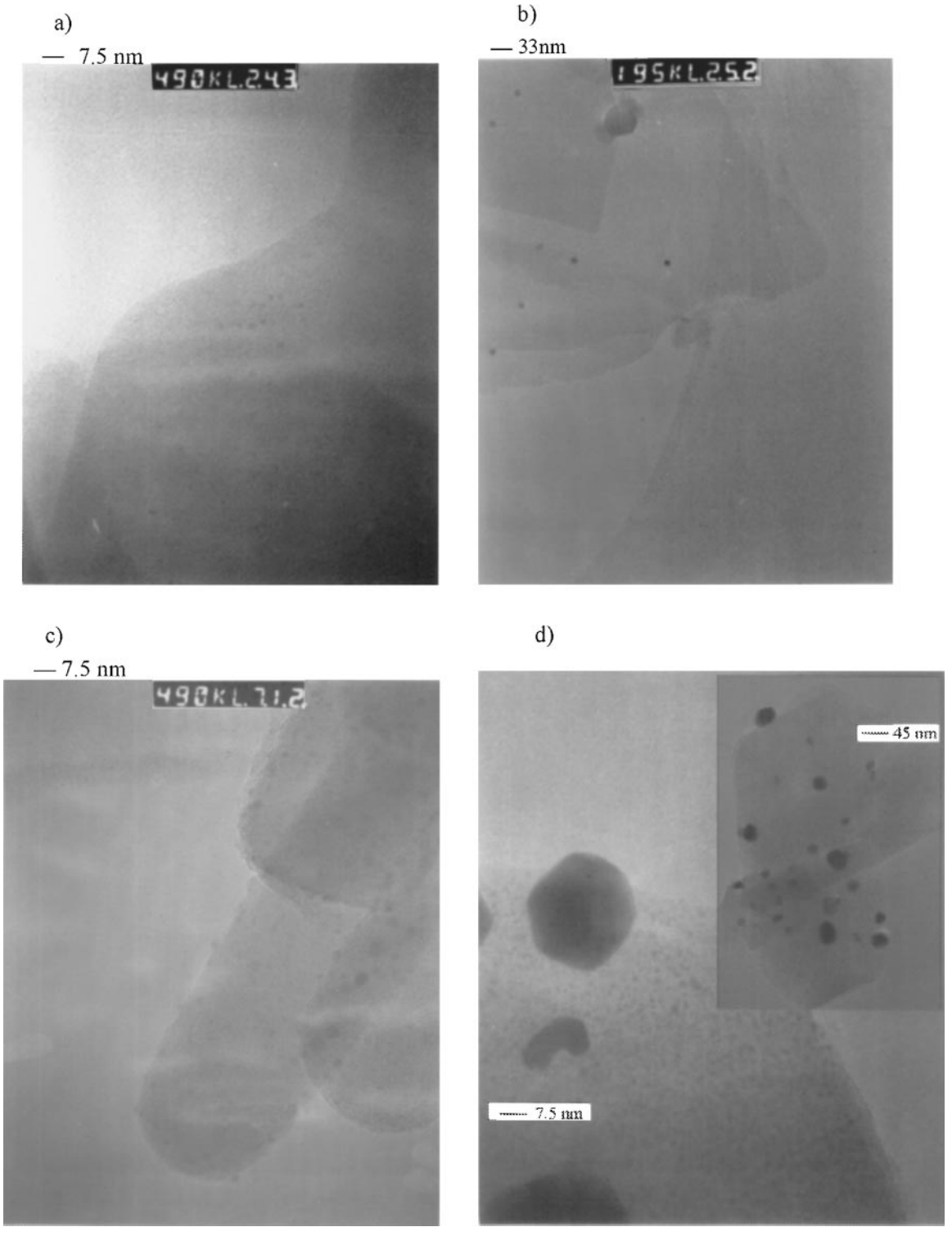

FIG. 1. HREM photographs of (a) 0.1% Pt–FER(17), (b) 0.1% Pt–FER(90), (c) 0.1% Pt–TON(72), and (d) 0.1% Pt–ZSM5(480).

TABLE 3

Initial Activity in the Hydrogenation of Ethene and 2,4,4-Trimethylpent-1-ene and the Fraction of Accessible Pt on the Outer Surface, as Calculated by the Ratio of the Two Rates

	Ethene		244TMPe		Accessible Pt on outer surface (%)
	Yield (%)	$r_{C_2H_4}$	Yield (%)	r_{TMPe}	
Pt–ZSM5(480)	12	3.3	1.9	2.3	20
Pt–ZSM5(125)	11	2.9	n.d.[a]	n.d.	n.d.
Pt–FER(17)	100	>30	0.5	0.6	<1
Pt–FER(90)	20	5.4	2.2	2.5	15
Pt–FER(670)	1	0.4	0.6	0.7	60
Pt–TON(35)	14	4.3	10.9	12.9	90
Pt–TON(72)	14	4.3	1.0	1.4	10
Pt–SiO_2	10[b]	1.2	3.3	4.0	100

Note: The hydrogenation rates $r_{C_2H_4}$ and r_{TMPe} are given in 10^{-4} mol/s g bar. Metal loading was 0.1 wt%.
[a] n.d. = not determined.
[b] 25 mg of catalyst instead of 10 mg.

activities, due to the different deactivation pattern of the various Pt–zeolites used. Therefore, only a comparison of the concentration of accessible Pt is reported here, but not absolute dispersion values.

Table 3 shows that the rate of ethene hydrogenation, i.e., the concentration of accessible Pt, decreased in the order Pt–FER(90) > Pt–TON > Pt–ZSM5 > Pt–SiO_2 ≫ Pt–FER(670). This trend is generally in line with the results of HREM. Note that for Pt–FER the dispersion strongly increased with the acid site concentration.

Large differences were also found in the rate of hydrogenation of 244TMPe. The catalytic activity decreased in the order Pt–TON(35) > Pt–SiO_2 > Pt–FER(90) ∼ Pt–ZSM5(480) > Pt–TON(72) > Pt–FER(670) ∼ Pt–FER(17), indicating a decreasing concentration of accessible Pt on the outer surface. Note that if large Pt particles are present on the outer surface of the zeolite, like in the case of Pt–ZSM5(480), the fraction of Pt on the outer surface will be high, but the fraction of accessible Pt atoms will be low.

If we assume that on the external surface of a material the same number of metal sites is accessible for ethene and for 244TMPe, it is possible to calculate the fraction of Pt sites located on the external surface from the ratio $q = r_{TMPe}/r_{C_2H_4}$. Pt–SiO_2 can be used as a reference, since the material is nonporous and all metal sites have to be located on the outer surface. The fraction of Pt sites on the external surface of the Pt–zeolites is then calculated from q(Pt–zeolite)/q(Pt–SiO_2). According to this estimation, most of the active Pt in TON(35) and FER(670) was located on the outer surface. For the other samples, i.e., Pt–ZSM5(480), Pt–TON(72), and Pt–FER(90), the fraction was between 10 and 20%. Due to the above-mentioned influence of the high acid site concentration on the ethene hydrogenation rate of Pt–FER(17) it was not possible to give a reliable value for the fraction of accessible Pt on the outer surface of this material. But the very low activity in the hydrogenation of 244TMPe indicated that most Pt was located in the pores.

For Pt–FER samples the fraction of accessible Pt on the outer surface decreased with increasing acid concentration, showing the stabilizing effect of acid sites on Pt particles in the pores. For Pt–TON, however, just the opposite effect was observed. Pt–TON(35) had most of the active Pt located on the outer surface, while Pt–TON(72) had only a small fraction. The different behavior could be related to the lower crystallinity of TON(35) compared to TON(72).

Skeletal Isomerization of 1-Butene

It has been mentioned above that the selectivity of a material in butene isomerization is an important criterion with respect to its suitability for dehydroisomerization. Therefore, the activity and selectivity of the parent zeolites in butene isomerization were studied (see Table 4). The activity in butene isomerization decreased in the order FER(17) > TON(72) ∼ TON(35) > ZSM5(480) > FER(90). As expected, FER was the most selective

TABLE 4

Comparison of Activity and Selectivity of ZSM5, TON, and FER in Butene Isomerization

Sample	ST (s g/m^3)	Yield i-$C_4^=$ (%)	k^a (m^3/s g)	Selectivity i-$C_4^=$ (%)
ZSM5(480)	5200	13.1	3.3×10^{-5}	87.1
TON(72)	4650	16.6	5.3×10^{-5}	86.8
TON(35)	4500	16.2	4.9×10^{-5}	88.6
FER(90)	4850	7.3	1.4×10^{-5}	94.3
FER(17)[b]	2400	14.8	9.2×10^{-5}	93.1

Conditions: 775 K, 1 bar, 100 min on stream. Feed: 7% 1-butene in Ar.
[a] Pseudo-first-order rate constant of butene isomerization.
[b] 4.5% 1-butene in the feed instead of 7%.

catalyst. It should, therefore, be most suited for dehydroisomerization.

Dehydroisomerization of n-Butane

The samples listed in Table 1 were tested for the dehydroisomerization of *n*-butane at 775 K. Figure 2 shows as an example the time-on-stream behavior of Pt–ZSM5(480), Pt–TON(35), and Pt–FER(90). Several important trends can be seen. (i) The dehydrogenation activity, i.e., the yield of $\sum C_4^=$, increased from Pt–FER(90) to Pt–TON(35) to Pt–ZSM5(480). The same trend was observed for the yield of isobutene. (ii) The dehydrogenation activity was stable for all three samples. (iii) The by-product spectra of the

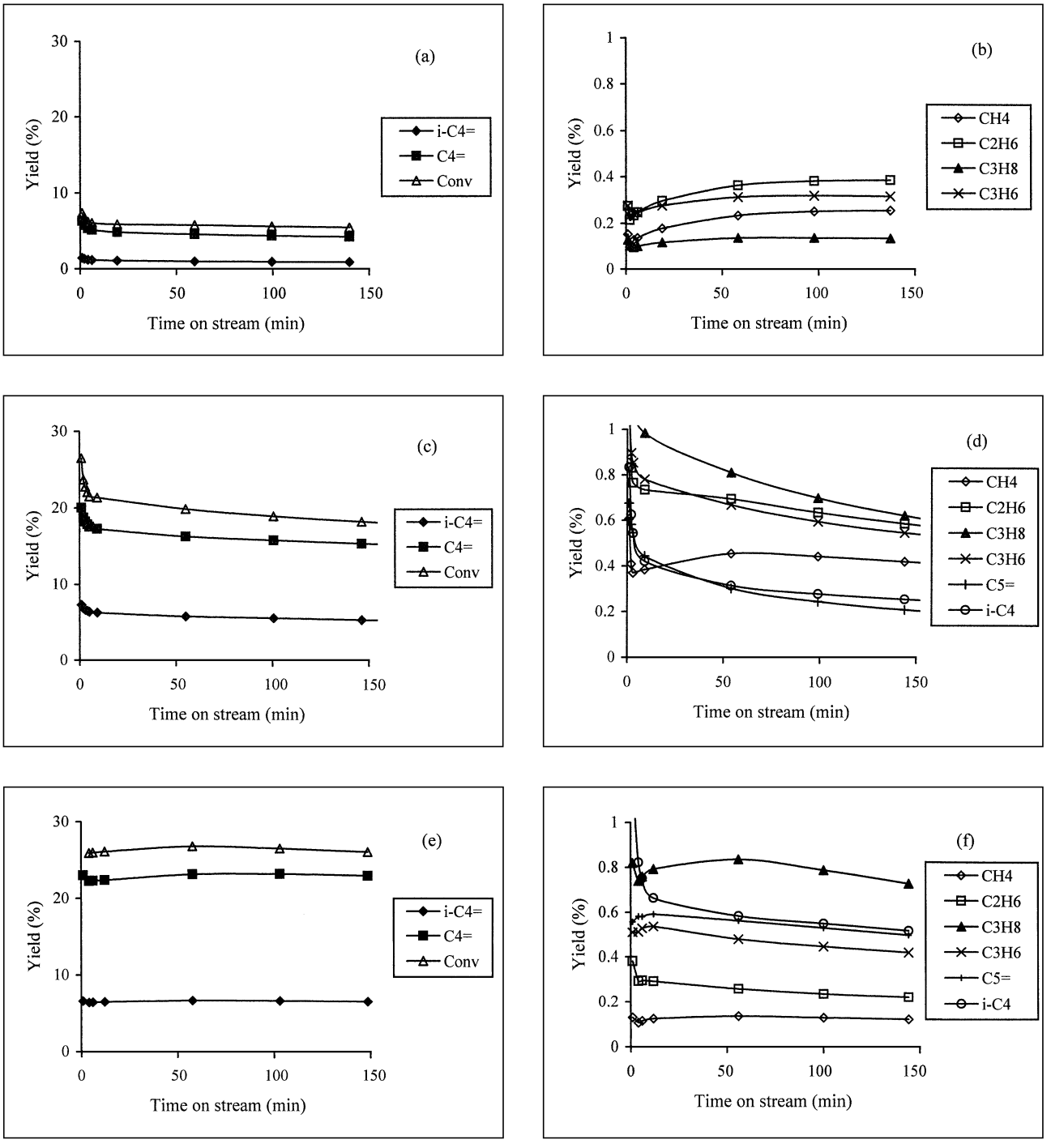

FIG. 2. Time-on-stream behavior in dehydroisomerization: (a, b) 0.1% Pt–FER(90), (c, d) 0.1% Pt–TON(35), and (e, f) 0.1% Pt–ZSM5(480). Conditions: 775 K, 1.0 bar, WHSV = 14 h^{-1}. Feed: 10% *n*-butane, 20% H_2, balance Ar.

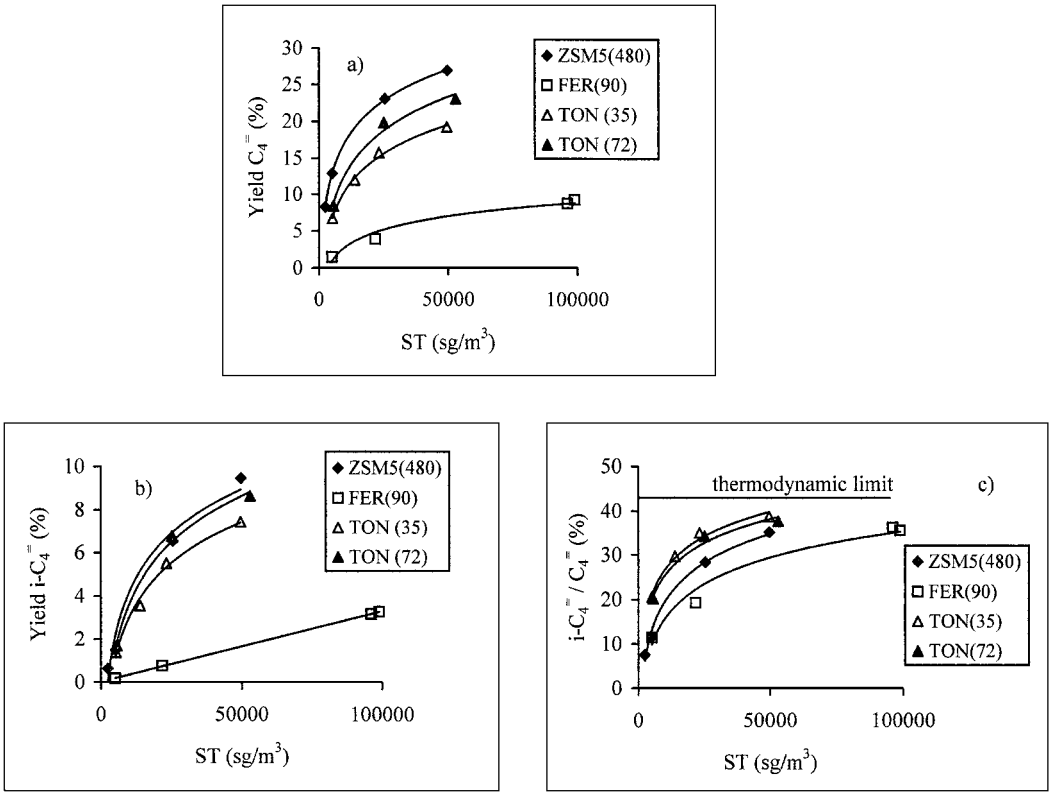

FIG. 3. Yields of (a) $\sum C_4^=$ and (b) i-$C_4^=$. (c) Ratio i-$C_4^=/\sum C_4^=$. All are shown as a function of space time ($ST = (dV/dt)/m_{cat}$, where (dV/dt) is the total flow in cubic meters per second at reactor temperature and pressure, and m_{cat} the mass of the catalyst in grams). Conditions: 775 K, 1.0 bar, 100 min on stream. Feed: 10% *n*-butane, 20% H_2.

three samples differed. In the case of Pt–FER(90), ethane was the most abundant by-product. With Pt–TON(35), almost equal amounts of propane, ethane, and propene were formed. In the case of Pt–ZSM5(480) propane and isobutane dominated.

As expected for the high reaction temperatures, also aromatic by-products (benzene and toluene) were formed, but the yield was rather low (<0.2%). Pt–FER released significantly lower amounts of aromatics than Pt–ZSM5 and Pt–TON, but the buildup of aromatics in the pores of Pt–FER could be observed by *in situ* IR spectroscopy.

Figure 3 shows the steady-state (after 100 min on stream) yields of the sums of butenes and of isobutene, as well as the ratio i-$C_4^=/\sum C_4^=$ as a function of space time. As also seen in Fig. 2, the dehydrogenation activity decreased in the order Pt–ZSM5(480) > Pt–TON(72) > Pt–TON(35) > Pt–FER(90). It leveled off at higher space times, caused by the approach of dehydrogenation equilibrium (the highest yield of $\sum C_4^=$ in Fig. 3 corresponds to about 75% of the equilibrium yield) and by kinetic inhibition due to adsorption of butenes on the metal sites (16).

The isomerization activities, i.e., the ratio i-$C_4^=/\sum C_4^=$, of both Pt–TON samples were higher than those of Pt–ZSM5 and Pt–FER. At low space times Pt–ZSM5 and both Pt–TON samples led to almost the same yield of isobutene. However, as isomerization approached thermodynamic equilibrium (at $ST > 25{,}000$ s g/m^3), the higher dehydrogenation activity of Pt–ZSM5 led to higher yields of isobutene than those obtained with Pt–TON.

Figure 4 shows the selectivity to dehydrogenation ($\sum C_4^=$) for the four samples. It increased in the order Pt–FER(90) $\ll$ Pt–TON(35) < Pt–TON(72) < Pt–ZSM5 (480).

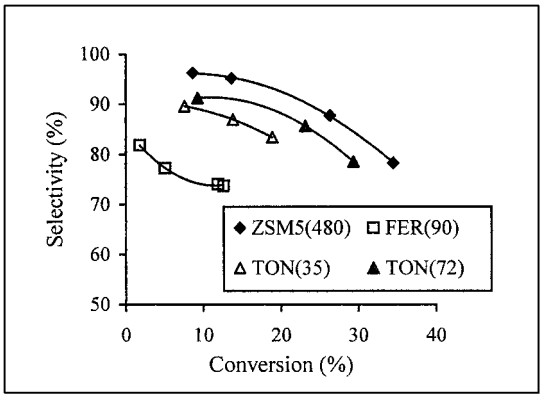

FIG. 4. Selectivity to $\sum C_4^=$ as a function of the conversion of *n*-butane. Conditions: 775 K, 1.0 bar, 100 min on stream. Feed: 10% *n*-butane, 20% H_2.

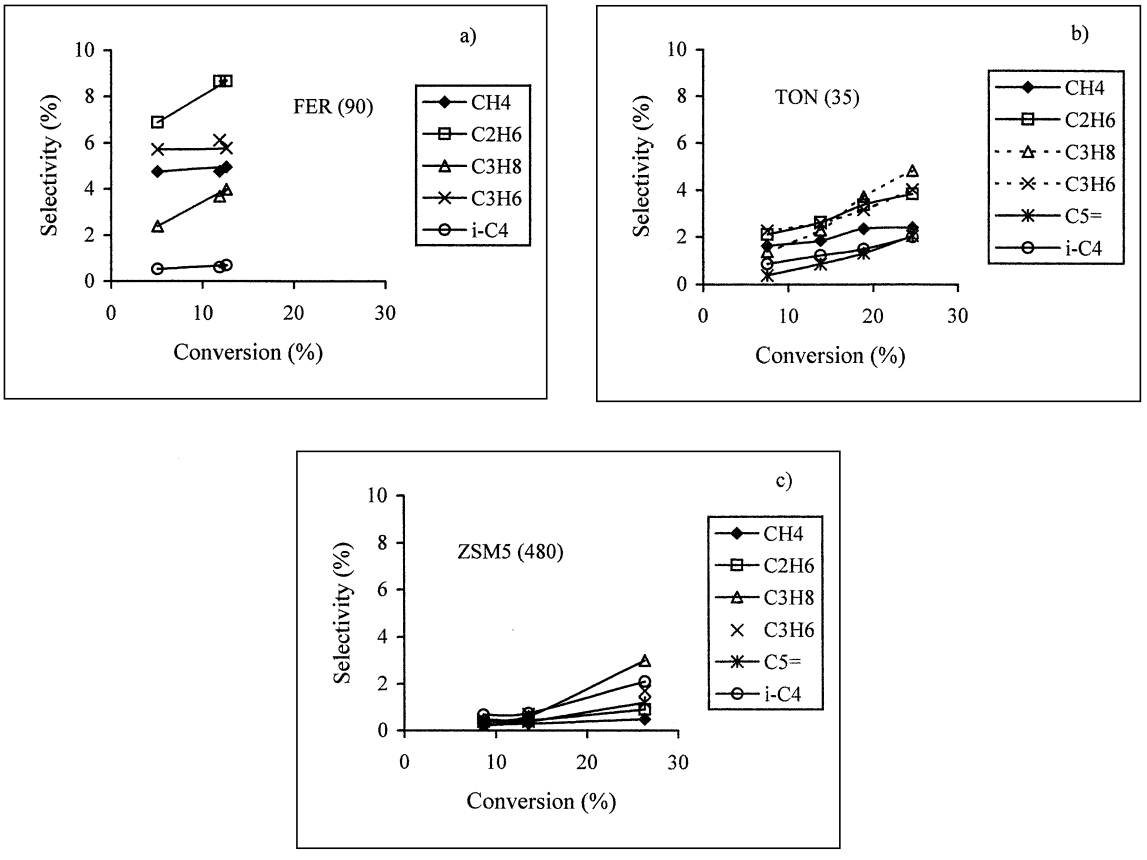

FIG. 5. Selectivity to the major by-products as a function of the conversion of *n*-butane: (a) Pt–FER(90), (b) Pt–TON(35), and (c) Pt–ZSM5(480). Conditions: 775 K, 1.0 bar, 100 min on stream. Feed: 10% *n*-butane, 20% H_2.

The by-product pattern is analyzed in more detail in Fig. 5. The by-products of Pt–ZSM5(480) originated almost exclusively from secondary reactions, as seen from the low selectivities at zero conversion. Pt–FER(90), on the other hand, showed a significant primary contribution of ethane, propene, methane, and propane (decreasing in that order). Pentene was not detected, indicating that oligomerization/cracking of butenes did not play a role in the by-product formation of Pt–FER.

Also in the case of Pt–TON the selectivites to methane, ethane, and propene had positive values at zero conversion, indicating that they were formed by primary reactions. The selectivity to these products was lower than that for Pt–FER, but higher than that for Pt–ZSM5. In contrast to Pt–FER, the formation of pentene was observed and its selectivity increased with conversion. Thus, oligomerization/cracking of butenes contributed to the by-product formation on Pt–TON like in the case of Pt–ZSM5.

In order to determine the contribution of protolytic cracking of butane to the byproduct formation on the three catalysts, the conversion of *n*-butane over the parent zeolites (Pt-free) was studied. *n*-butane was converted to cracking products, according to the reactions [1] and [2], to isobutane [3], and to an equilibrium mixture of butenes [4].

$$n\text{-}C_4H_{10} \rightarrow CH_4 + C_3H_6 \quad [1]$$

$$n\text{-}C_4H_{10} \rightarrow C_2H_6 + C_2H_4 \quad [2]$$

$$n\text{-}C_4H_{10} \rightarrow i\text{-}C_4H_{10} \quad [3]$$

$$n\text{-}C_4H_{10} \rightarrow C_4H_8 + H_2 \quad [4]$$

Table 5 compiles the rates of formation of C_1–C_3 hydrocarbons for the parent and the Pt–zeolites. For the parent zeolites the rates of methane and propane and of ethane and ethene formation matched exactly, as expected from the stoichiometry of reactions [1] and [2]. In the case of the Pt–zeolites alkanes and alkenes can be interconverted by hydrogenation/dehydrogenation on the metal (1). Therefore, it is better to compare the total rate of alkane and alkene formation in the presence and in the absence of Pt. These values are listed in Table 6. The ratio of the rates shows that in the case of Pt–ZSM5(480) and Pt–TON(35) the by-product formation was significantly higher than that for the parent zeolites. This suggests that the contribution of protolytic cracking to the overall by-product formation is small. Also in the case of Pt–FER(90) the by-product formation was much higher than that for the parent. In contrast to Pt–ZSM5 and Pt–TON, however, the increased

TABLE 5

Rate of By-product Formation ($\times 10^7$ mol/s g) over the Parent Zeolites and the Pt–Zeolites (0.1 wt% Pt)

	ZSM5(480)	Pt–ZSM5(480)	TON(35)	Pt–TON(35)	FER(90)	Pt–FER(90)	FER(17)	Pt–FER(17)
CH_4	0.50	3.3	1.2	12	0.60	6.7	11	29
C_2H_6	0.25	3.1	1.4	8.9	0.60	5.1	10	26
C_2H_4	0.25	0.15	1.4	0.6	0.60	0.76	10	1.4
C_3H_8	0.00	6.8	0.0	6.5	0.017	1.2	0.22	2.7
C_3H_6	0.50	3.9	1.2	5.6	0.59	2.8	10	8.2

Conditions: WHSV = 14 h^{-1} (ST = 25,000 m^3/s g), 775 K, 1.0 bar, 100 min on stream. Feed: 10% *n*-butane, 20% hydrogen, balance Ar.

by-product formation was due to an increase in protolytic cracking itself, as will be discussed later.

For Pt–FER the effect of the SiO_2/Al_2O_3 ratio was studied over a wide range from 17 to 670. Table 7 compares the results obtained with the three samples. With decreasing SiO_2/Al_2O_3 ratio (with increasing acid site concentration) the conversion of *n*-butane and the ratio i-$C_4^=/\sum C_4^=$ increased. The increased conversion was due to an increased by-product formation. The yield of $\sum C_4^=$, however, decreased. For Pt–FER(17) the by-product formation was on the same order of magnitude as that for the parent FER(17) (see Tables 5 and 6). Thus, the contribution of protolytic cracking to the overall by-product formation of Pt–FER(17) was very high.

Figure 6 shows the dependence of the rate of by-product formation on the Al content of the Pt–FER samples. The rate of methane and ethane formation increased almost linearly with Al content, as expected if methane and ethane originate from protolytic cracking on the Brønsted acid sites. The rate of C_3 formation, however, did not increase in parallel with the formation of methane, as predicted by the stoichiometry of reaction [1]. Thus, a significant part of the methane formation (and probably also the ethane formation, since the curves were parallel) must be due to hydrogenolysis and not to protolytic cracking. Note that the contribution of hydrogenolysis, represented by the difference in the rates of methane and C_3 formation in Fig. 6, increased with the acid site concentration of the zeolite.

Increasing the metal loading of Pt–FER(17) from 0.1 to 0.3 wt% Pt led to a drastic increase in the formation of methane and ethane (see column 4 of Table 7), indicating that mainly hydrogenolysis took place with this sample. The yield of $\sum C_4^=$ was only 1.9%.

TABLE 6

Ratio of the Rates of C_1–C_3 Formation (Alkane + Alkene) in the Presence and in the Absence of Pt (0.1 wt%)

	ZSM5(480)	TON(35)	FER(90)	FER(17)
C_1	6.6	10.0	11.1	2.6
C_2	6.5	3.4	4.9	1.4
C_3	21.4	10.1	6.6	1.1
$\sum nC_n$	14	6.5	6.3	1.4

Conditions: WHSV = 14 h^{-1} (ST = 25,000 m^3/s g), 775 K, 1.0 bar, 100 min on stream. Feed: 10% *n*-butane, 20% hydrogen, balance Ar.

DISCUSSION

FER allows significantly higher selectivities to be achieved for the skeletal isomerization of *n*-butene to isobutene than TON and ZSM5. In dehydroisomerization of *n*-butane, however, the selectivity to by-products (i.e., products other than $C_4^=$) decreased in the order Pt–FER(90) > Pt–TON(35) > Pt–ZSM5(480). The by-product pattern of the three catalysts (see Fig. 5) showed that with Pt–TON and especially with Pt–FER a large fraction of the by-products was of primary nature, in contrast to Pt–ZSM5(480) where most of the by-products were formed by secondary reactions. The selectivity to primary by-products (i.e., the selectivity to by-products extrapolated to zero conversion) increased from Pt–ZSM5(480) (<4%) to Pt–TON(35) (~9%) to Pt–FER(90) (~17%) (see Fig. 4). While oligomerization/cracking of butenes was the only relevant side reaction with Pt–ZSM5(480), its contribution was negligible with Pt–FER(90). Pt–TON(35) was an intermediate case. Both primary and secondary side reactions occurred with this catalyst.

TABLE 7

Yield of Major Products in the Dehydroisomerization of *n*-Butane over Pt–FER

SiO_2/Al_2O_3	670	90	17	17
wt% Pt	0.1	0.1	0.1	0.3
CH_4	0.01	0.24	1.06	13.4
C_2H_6	0.01	0.35	1.92	6.4
C_2H_4	0.01	0.05	0.09	0.18
C_3H_8	0.00	0.12	0.30	0.88
C_3H_6	0.02	0.29	0.90	0.40
i-$C_4^=$	0.04	0.75	1.04	0.75
$\sum C_4^=$	4.7	3.9	3.4	1.9
Conversion	4.9	5.1	7.7	25
i-$C_4^=/\sum C_4^=$	0.8	19	31	39

Conditions: WHSV = 14 h^{-1}, 775 K, 1.0 bar, 100 min on stream. Feed: 10% *n*-butane, 20% H_2.

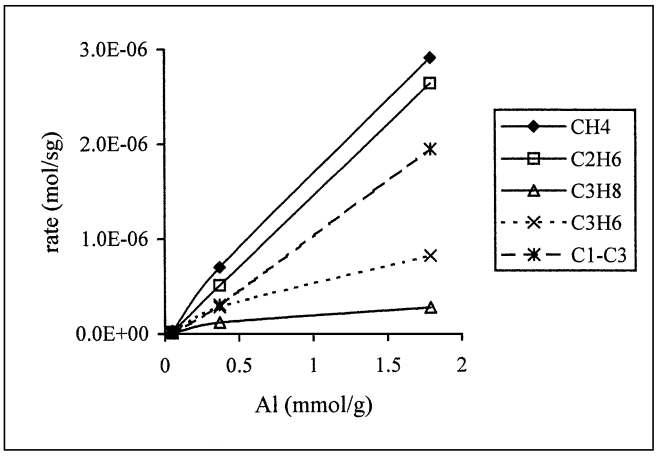

FIG. 6. Rate of by-product formation as a function of the Al content of Pt–FER. Conditions: WHSV = 14 h^{-1}, 775 K, 1.0 bar, 100 min on stream. Feed: 10% *n*-butane, 20% H_2.

We conclude, thus, that suppressing oligomerization/cracking reactions of the butenes is not sufficient for improving the selectivity of a catalyst for dehydroisomerization of *n*-butane. The other side reactions (1), protolytic cracking of *n*-butane on the acid sites and hydrogenolysis of *n*-butane on the metal sites, have to be minimized, as well.

The Contribution of Protolytic Cracking of n-Butane

Provided that the rate of protolytic cracking is constant in the presence and in the absence of Pt, protolytic cracking accounted for 9% (on a carbon basis) of the light by-products (C_1–C_3) in the case of Pt–ZSM5(480) and for 15–16% in the case of Pt–TON(35). With Pt–ZSM5(480) and Pt–TON(35), the other light hydrocarbons were formed by hydrogenolysis and oligomerization/cracking. In the case of Pt–FER(90), however, we had concluded from the absence of pentene in the products that oligomerization/cracking did not take place. The increase in the formation of propene (see Table 5) must, therefore, be due to an increase in protolytic cracking in the presence of Pt. Thus, most of the light by-products of Pt–FER(90) were formed by cracking of *n*-butane.

For the overall selectivity in dehydroisomerization the relative rates of the two parallel reactions, protolytic cracking and dehydrogenation, are important. The corresponding rate constants and their ratio are given in Table 8. The ratio k_{dehyd}/k_{crack} was inversely proportional to the selectivity to C_3H_6 (at zero conversion), which was taken as a measure of the selectivity to protolytic cracking.[2] Note that the increase in selectivity to protolytic cracking from Pt–ZSM5 to Pt–TON to Pt–FER was caused by the increase in the rate of cracking *and* the decrease in the rate of hydrogenation in this order.

The higher cracking activity of TON and FER compared to that of ZSM5 was attributed to the higher acid site concentrations of these samples. In dehydroisomerization over Pt–TON and Pt–FER, the initial selectivity to propene at zero conversion decreased with increasing SiO_2/Al_2O_3 ratio, showing that the selectivity to protolytic cracking could be reduced by reducing the acid site concentration. But since butene isomerization is also acid catalyzed, the acid site concentration cannot be reduced beyond a certain limit. Pt–FER(670), for example, had a very low activity for protolytic cracking, but also hardly any activity in butene isomerization. In general a material will be more suited for dehydroisomerization the higher its activity for butene isomerization is compared to its activity for protolytic cracking. The ratio k_{isom}/k_{crack} decreased in the order ZSM5(480) > TON(72) > TON(35) > FER(90) > FER(17). We can also see from Table 8 that the rate of protolytic cracking depended more strongly on the concentration of acid sites than on the rate of butene isomerization. Thus, materials with high SiO_2/Al_2O_3 should be more suited for dehydroisomerization.

Also the strength of acid sites could play a role in the selectivity to cracking. Microcalorimetric measurements indicated, however, that there is no significant difference between the strength of acid sites in ZSM5, TON, and FER (24). This is in line with the next-nearest neighbor theory, which predicts that above a certain SiO_2/Al_2O_3 ratio (19 for ZSM5, Ref. 25) the intrinsic strength of a Brønsted acid site is constant (26, 27). Since all our samples are above or close to this critical SiO_2/Al_2O_3 ratio we believe that only the concentration of Brønsted acid sites has to be taken into account to explain our results. Regarding Lewis acidity, we do not have any evidence that it plays an important role in the reaction.

The Contribution of Hydrogenolysis

It is difficult to distinguish the contribution of hydrogenolysis from protolytic cracking of *n*-butane and from oligomerization/cracking of butenes. In the presence of Pt and hydrogen the alkenes formed by cracking can be hydrogenated to the corresponding alkanes. As a result, ethane and propane can be formed via all three reaction routes. In order to estimate the contribution of hydrogenolysis, let us turn to the elementary reaction steps. If only protolytic cracking and oligomerization/cracking take place, the molar ratio C_1/C_3 must be ≤ 1 (=1 if only protolytic cracking takes place, see Eq. [1]; <1 if C_3 is also formed by oligomerization/cracking). On the other hand, methane is the main product of hydrogenolysis at the high reaction temperatures applied, next to only small amounts of ethane and

[2] In contrast to the suggestion of Haag and Dessau (23) to use the paraffinic products for analyzing the rate of protolytic cracking we used propene, because the paraffins methane and ethane can also be formed by hydrogenolysis. The contribution of secondary reactions to the formation of propene was eliminated by extrapolation of the selectivity to zero conversion.

TABLE 8

Pseudo-First-Order Rate Constants of Protolytic Cracking (k_{crack}) and Dehydrogenation of *n*-butane (k_{dehyd}) as Well as of Skeletal Isomerization of 1-Butene (k_{isom})

	k_{crack}[a] (10^{-7} m^3/s g)	k_{isom} (10^{-5} m^3/s g)	k_{dehyd}[b] (10^{-5} m^3/g)	k_{dehyd}/k_{crack}	Selectivity C_3H_6 (%)[c]
(Pt–)ZSM5(480)	0.43	3.3	5.0 ± 0.5	1150	0.1 ± 0.1
(Pt–)TON(72)	0.8	5.3	2.2 ± 0.2	275	1.5 ± 0.1
(Pt–)TON(35)	1.7	4.9	1.8 ± 0.2	105	2.1 ± 0.1
(Pt–)FER(90)	0.74 (4.3[d])	1.4	0.3 ± 0.1	40 (7[d])	5.7 ± 0.3
(Pt–)FER(17)	130	9.2	<0.3	<0.2	~30

Note. The ratio k_{dehyd}/k_{crack} is correlated to the selectivity to protolytic cracking, represented by the selectivity to propene at zero conversion.

[a] k_{crack} was determined from the rate of protolytic cracking over the parent zeolite.

[b] k_{dehyd} was calculated according to the method described in Ref. (16) and extrapolated to zero conversion.

[c] Selectivity was extrapolated to zero conversion.

[d] Since the Pt–FER(90) had a significantly higher activity than the parent (see text), its cracking rate was estimated from $r_{C_3} + 0.5 r_{C_2}$. The value is given in parentheses.

propane (the selectivity to methane in hydrogenolysis increases with temperature, Ref. 28). Hence, we can use the difference in the rate of methane formation and the rate of C_3 formation (propane and propene) as a measure of the hydrogenolysis activity. Especially at low conversions, when the contribution of oligomerization/cracking to the C_3 formation is low, the difference $r_{CH_4} - r_{C_3}$ should give a good estimate of the rate of hydrogenolysis.

Using this approach, the initial selectivity to hydrogenolysis (extrapolated to zero conversion) and the reaction rate were estimated. The results are compiled in Table 9. The rate of hydrogenolysis increased from Pt–FER(90) to Pt–TON (both SiO_2/Al_2O_3 ratios comparable) to Pt–FER(17) (due to the large relative error margin of the extrapolation a rate could not be given for Pt–ZSM5(480)). The selectivity to hydrogenolysis, which is determined by the relative rates of dehydrogenation and hydrogenolysis, increased from Pt–ZSM5(480) to Pt–TON (both) to Pt–FER(90) to Pt–FER(17).

The Effect of the Zeolite on the Metal Activity

The results discussed so far showed a very peculiar behavior of Pt–FER. In contrast to Pt–ZSM5 and Pt–TON, it had a very low activity for dehydrogenation and a high selectivity to hydrogenolysis, especially in the case of Pt–FER(17). The high selectivity of Pt–FER(17) to hydrogenolysis was attributed to two factors. First of all, hydrogenolysis is a structure-sensitive reaction and its TOF increases with decreasing particle size (21, 28–31). Dehydrogenation is structure insensitive (32) and its TOF is independent of the particle size. Thus, the selectivity to hydrogenolysis is expected to be higher for small Pt particles. Indeed, Pt–FER(17) had the smallest Pt particles found by HREM and the highest selectivity to hydrogenolysis, while Pt–ZSM5(480) had the largest particles and the lowest selectivity to hydrogenolysis. But a second effect seems to play a role, as well. Comparing Tables 8 and 9, a correlation between hydrogenolysis and protolytic cracking is noted. The rates of both reactions are low on Pt–ZSM5(480), average on Pt–TON, and high on FER(17). Among the Pt–FER materials an increase of hydrogenolysis with the Al content was observed. This could be due to the observed decrease in Pt particle size with increasing Al content (see the dispersion data in Table 3). But it is also possible that a synergy between cracking and hydrogenolysis exists, as proposed in Ref. (33). Alkenes formed by cracking (i.e, ethene and/or propene) are strongly adsorbed on the Pt particles. When the metal particles are small and the activity for hydrogenolysis is, therefore, high (see above), hydrogenolysis of the adsorbed alkenes to methane takes place. Via this synergetic effect the high cracking activity of Pt–FER(17) also leads to a further increase of the formation of hydrogenolysis products.

The large difference in dehydrogenation activity, which decreased from Pt–ZSM5 to Pt–TON to Pt–FER, is more difficult to understand. The HREM measurements indicate that the different dehydrogenation activity was not primarily related to the metal dispersion. Pt–ZSM5(480) exhibited only a moderate dispersion, but the highest

TABLE 9

Rate of Hydrogenolysis (Estimated by $r_{CH_4} - r_{C_3}$) and Selectivity to hydrogenolysis[a]

	Rate (10^{-7} mol/s g)	k_{dehyd}/k_{hydr}	Selectivity (%)
Pt–ZSM5(480)	n.d.	n.d.	0.1 ± 0.1
Pt–TON(72)	5.7 ± 0.5	60	0.6 ± 0.1
Pt–TON(35)	6.0 ± 0.5	50	0.6 ± 0.1
Pt–FER(90)	3.5 ± 0.3	15	2.5
Pt–FER(17)	20	<2.5	>5

[a] Both were extrapolated to zero conversion.

dehydrogenation activity, while Pt–FER(90) had a rather high dispersion, but a very low dehydrogenation activity. Interestingly, the differences between Pt–ZSM5, Pt–TON, and Pt–FER were much larger than the differences within one zeolite family. For both Pt–TON and all three Pt–FER materials similar dehydrogenation rates were found. Thus, the different metal activity was related more to the differences in framework structure and morphology of ZSM5, FER, and TON than to a variation in the SiO_2/Al_2O_3 ratio. This suggests that the different behavior of the Pt–zeolites may be related to diffusion of reactants and products. ZSM5 has a two-dimensional pore system and diffusion of the reactants and products is easier than in FER and TON, which have a one-dimensional channel system (the channel system of FER is two-dimensional, but most molecules cannot pass the eight-membered ring channels). The pores are narrower than those of ZSM5, and even more so when Pt particles are present within the channel. It is, thus, possible that pore diffusion of the reactants and/or products is the rate-limiting step in Pt–TON and Pt–FER.

The rates of diffusion in Pt–TON and Pt–FER, however, should be quite similar and this cannot explain why Pt–TON was about 6 times more active for dehydrogenation than Pt–FER. This difference was attributed to the morphology of the samples. The crystals of Pt–FER(90) were larger than those of Pt–TON (see Table 2). A large concentration of small zeolite particles was found next to the well-shaped needles in both Pt–TON materials. Thus, on average the length of the pores was shorter in Pt–TON than in Pt–FER, thereby reducing the diffusion path length and the negative effect on the reaction rate. Pt–FER(17), on the other hand, had crystals of comparable size to the two Pt–TON materials. On this sample the low concentration of Pt on the outer surface, as a result of which most of the dehydrogenation has to take place in the pores, in combination with the high acid site density could make product desorption the rate-limiting step.

CONCLUSIONS

While in the dehydroisomerization of *n*-butane over Pt–ZSM5(480) the selectivity was almost exclusively determined by the extent of oligomerization/cracking reactions, protolytic cracking and hydrogenolysis had a significant contribution to the by-product spectrum in the cases of Pt–TON(35 and 72) and Pt–FER(17 and 90). The selectivity to protolytic cracking was inversely proportional to the ratio k_{dehyd}/k_{crack}. Thus, a high ratio of k_{dehyd}/k_{crack} is an important design parameter for a dehydroisomerization catalyst. The contribution of protolytic cracking can be reduced by increasing the SiO_2/Al_2O_3 ratio. But since butene isomerization is also acid catalyzed, the increase in SiO_2/Al_2O_3 cannot be unlimited and an optimum has to be found. In general, zeolites with a high TOF for butene isomerization and a low TOF for protolytic cracking should be better suited as dehydroisomerization catalysts. Since protolytic cracking shows a stronger dependence on the concentration of acid sites than butene isomerization, materials with low acid site concentrations give better selectivities in dehydroisomerization.

Surprisingly, the dehydrogenation activity of the Pt–zeolites is not primarily related to the metal dispersion. Pt–ZSM5(480) with a moderate dispersion and a very inhomogeneous distribution of the metal gave the best results, while the opposite was the case for Pt–FER(17), which had a very homogeneous distribution of small particles mainly located in the zeolite pores. The zeolite framework, on the other hand, has a large influence on the dehydrogenation activity, which decreases significantly from Pt–ZSM5 to Pt–TON to Pt–FER. This is tentatively attributed to diffusion control. The presence of small metal particles located in the narrow pores of large zeolite crystals is undesirable for dehydroisomerization, since it enhances the diffusional constraints.

ACKNOWLEDGMENTS

This work was performed under the auspices of NIOK, the Netherlands Institute of Catalysis Research. IOP Katalyse (IKA 94023) is gratefully acknowledged for financial support. M. J. G. Janssen, from Exxon Chemical International Inc., Basic Chemicals Technology Europe, and G. Kinger, from the Technical University of Vienna, are thanked for supplying the FER and TON samples. The HREM measurements were performed and analyzed by Dr. P. Kooyman at the National Center for HREM, Delft.

REFERENCES

1. Pirngruber, G. D., Seshan, K., and Lercher, J. A., *J. Catal.* **186**, 188 (1999).
2. O'Young, Ch.-L., Pellet, R., Casey, D., Ugolini, J., and Sawicki, R. A., *J. Catal.* **151**, 467 (1995).
3. Mooiweer, H. H., de Jong, K. P., Kraushaar-Czarnetzki, B., Stork, W. H. J., and Krutzen, B. C. H., *in* "Zeolites and Related Microporous Materials: State of the Art 1994" (J. Weitkamp, H. G. Karge, H. Pfeifer, and H. Hölderich, Eds.), Stud. Surf. Sci. Catal., Vol. 84, p. 2327. Elsevier, Amsterdam, 1994.
4. Xu, W.-Q., Yin, Y.-G., Suib, St. L., Edwards, J. C., and O'Young, Ch.-L., *J. Phys. Chem.* **99**, 9443 (1995).
5. Guisnet, M., Andy, P., Gnep, N. S., Benazzi, E., and Travers, C., *J. Catal.* **158**, 551 (1996).
6. Simon, M. W., Suib, S. L., and O'Young, Ch.-L., *J. Catal.* **147**, 484 (1994).
7. Byggningsbacka, R., Lindfors, L.-E., and Kumar, N., *Ind. Eng. Chem. Res.* **36**, 2990 (1997).
8. Xu, W.-Q., Yin, Y.-G., Suib, St. L., and O'Young, Ch.-L., *J. Catal.* **150**, 34 (1994).
9. Gajda, G. J., U.S. Patent 5.132.484 (1992), assigned to UOP.
10. Gielgens, L. H., Veenstra, I. H. E., Ponec, V., Haanepen, M. J., and van Hooff, J. H. C., *Catal. Lett.* **32**, 195 (1995).
11. Asensi, M. A., Corma, A., and Martinez, A., *J. Catal.* **158**, 561 (1996).
12. Grandvallet, P., de Jong, K. P., Mooiweer, H. H., Kortbeek, A. G. T., and Kraushaar-Czarnetzki, B., EP Patent 501.577 (1992), assigned to Shell Internationale Research Maatschappij B.V.

13. Barri, S. A. I., Walker, D. W., and Tahir, R., EP Patent 247.802 (1990), assigned to The British Petroleum Co.
14. Ernst, S., Weitkamp, J., Martens, J., and Jacobs, P., *Appl. Catal.* **48**, 137 (1989).
15. Pirngruber, G. D., Seshan, K., and Lercher, J. A., *J. Catal.* **190**, 338 (2000).
16. Pirngruber, G. D., Seshan, K., and Lercher, J. A., *J. Catal.* **190**, 396 (2000).
17. Cortright, R. D., Goddard, S. A., Rekoske, J. E., and Dumesic, J. A., *J. Catal.* **127**, 342 (1991).
18. Houzvicka, J., Klik, R., Kubelkova, L., and Ponec, V., *Catal. Lett.* **43**, 7 (1997).
19. Benesi, H. A., Curtis, R. M., and Studer, H. P., *J. Catal.* **10**, 328 (1988).
20. Degussa, Schriftenreihe Pigmente, "Aerosil, Aluminiumoxid C und Titandioxid P25 für Katalysatoren," No. 72.
21. Schlatter, J. C., and Boudart, M., *J. Catal.* **24**, 482 (1972).
22. Che, M., and Bennett, C. O., *Adv. Catal.* **36**, 55 (1989).
23. Haag, W. O., and Dessau, R. M., *in* "Proceedings 8th International Congress on Catalysis, Berlin, 1984," Vol. 2, p. 305. Dechema, Frankfurt-am-Main, 1984.
24. Pieterse, J. A. Z., Ph.D. thesis, University of Twente, Enschede, The Netherlands, 1999.
25. Barthomeuf, D., *in* "Catalysis," p. 177. Elsevier, Amsterdam, 1987.
26. Mortier, W. J., *J. Catal.* **55**, 138 (1978).
27. Jacobs, P. A., *Catal. Rev.-Sci. Eng.* **24**, 415 (1982).
28. Bond, G. C., and Gelsthorpe, M. R., *J. Chem. Soc., Faraday Trans. 1* **85**, 3767 (1989).
29. Bond, G. C., Calhoun, J., and Hooper, A. D., *J. Chem. Soc., Faraday Trans.* **92**, 5117 (1996).
30. Rodriguez-Reinoso, F., Rodriguez-Ramos, I., Moreno-Castilla, C., Gruerrero-Ruiz, A., and Lopez-Gonzalez, J. D., *J. Catal.* **107**, 1 (1987).
31. Campbell, R. A., Guan, J., and Mady, T. E., *Catal. Lett.* **27**, 273 (1994).
32. Biloen, P., Dautzenberg, F. M., and Sachtler, W. M. H., *J. Catal.* **50**, 77 (1977).
33. Dowden, D. A., *in* "Catalysis" (C. Kemball and D. A. Dowden, Eds.), Vol. 2, p. 21. The Chemical Society, London, 1977.